UDC 532.516:536.24.01

A. KHALATOV[1], A. BYERLEY[2]

[1]Institute for Engineering Thermophysics, National Academy of Sciences, Kiev, Ukraine
[2]United States Air Force Academy, Colorado Springs, USA

EFFECT OF PRE-DIMPLE BOUNDARY LAYER THICKNESS ON FLOW CHARACTERISTICS WITHIN AND DOWNSTREAM OF A SINGLE SHALLOW DIMPLE

Досліджено особливості осередненої та нестаціонарної структури потоку перед, всередині і за дрібними заглибленнями циліндричної та сферичної форми, які зроблені на плоскій пластині на різних відстанях від входу, що забезпечує різну товщину пограничного шару набігаючого потоку. Порівняно характеристики заглиблень циліндричної та сферичної форми.

Исследованы особенности осредненной и нестационарной структуры потока перед, внутри и за "мелким" углублением цилиндрической и сферической формы, выполненным на плоской пластине на различных расстояниях от входа, что обеспечивает различную толщину пограничного слоя набегающего потока. Сделано сравнение характеристик углублений цилиндрической и сферической формы.

This study is to investigate the details of the average and unsteady flow structures in front, inside and downstream of the shallow spherical and cylindrical dimple placed on a flat plate at the different distances with different pre-dimple boundary layer thicknesses. A comparison of both spherical and cylindrical dimple geometric configurations was made to assess their relative benefits.

C_f – drag coefficient;
D – dimple projected (surface) diameter, m;
f – frequency of bulk flow oscillations, s^{-1};
f_1 – flow gradient parameter, $\delta_2 [\partial U_\infty / \partial x] / U_\infty$;
H* – channel height, m;
H – shape factor, δ_1 / δ_2 ;
h – dimple depth, m;
L – extent of in-dimple separation zone, m;
Re_D – Reynolds number based, $U_\infty D/\nu$;
Re_x – Reynolds number, $U_\infty x/\nu$;
SCD – single cylindrical dimple;
Sh – Strouhal number, $f D / U_\infty$;
x – distance from test section beginning to dimple front edge (over centerline), m;
x* – downstream distance from dimple back rim, m;
x_D – pre-dimple measurements, m;
U_∞ – flow speed in front of dimple, m/s;
z – spanwise distance, m.

Greek symbols:

δ – boundary layer thickness, m;
δ_{0av} – average boundary layer thickness, m;
δ_2 – momentum thickness, m;
δ_1 – displacement thickness, m;
ν – air kinenatic viscosity, m^2/s.

Subscripts:

o – flow parameters in front of a dimple;
oo – flow parameters over a flat plate.

INTRODUCTION

The suction side of turbine blades suffers from the boundary layer separation while operating at low (off-design) Reynolds numbers. The separation zone reduces the blade efficiency and leads to a reduction of turbine power. To improve the turbine efficiency both active and passive flow control techniques are now being considered. Amongst the potential passive techniques are shallow surface dimples ($h/D \approx 0{,}10$) since they provide reduced profile losses at low Reynolds numbers [1, 2]. Compared with other passive techniques (V-grooves; wires), spherical dimples have demonstrated the best results in terms of reduction in separation losses and improvements in the region of a flow reattachment. The best condition for the flow reattachment creates the turbulent flow pattern both inside and downstream of the dimple [1].

The spherical dimples can be classified based on their depth to diameter ratio: (a) shallow dimples

(h/D≤ 0,06...0,10), (b) deep dimples (h/D>0,2), and (c) intermediate depth dimples (h/D = 0,1...0,2). There is no separation inside shallow dimples, where only Gцrtler vortices exist over a dimple concavity generating the Karman vortex streets downstream of the dimple [3 – 6]. Analysis of the Russian data shows that in the intermediate and deep dimples the Karman vortex street appears at Re_D from 600 to 800 and transforms into the twin vortex pattern between $Re_D \approx 1000$ and $Re_D \approx 3200$. In some cases inside the intermediate dimple the twin vortex may exist up to $Re_D = 100000$ [10].

The twin vortex was observed in the intermediate spherical dimples (h/D = 0,15 ... 0,20) in the Re_D range between 3200 and 13000 however this vortex disappeared between 11000 and 27000 creating the side-to-side fluctuating vortex [9]. Gachechiladze [7] has reported the existence of a twin vortex in the intermediate dimple (h/D = 0,15) up to $Re_D \approx 4000$; the weak side-to-side fluctuating vortex appears at $Re_D \approx 4000$ to transform into the stable fluctuating vortex structures by $Re_D \approx 5500$.

Kesarev & Kozlov [12] have reported the existence of developed fluctuating vortex structures inside a deep single hemispherical dimple (h/D=0,5) at high Reynolds numbers. At $Re_D > 180000$ and low freestream turbulence, the Strouhal number is 0,08 (16 Hz). At higher freestream turbulence the vortex fluctuations are suppressed. The Strouhal number is 0,04 (8 Hz) at Tu =15 % and drops to Sh = 0,006 (0,13 Hz) at Tu = 20 % (Re_D = 300000). Furthermore, the external vorticity greatly reduces the vortex fluctuations inside the dimple. The oscillating flow structures inside the hemispherical dimple (h/D = 0,5) were also observed in Snedeker and Donaldson [13] at Re_D from 73000 to 320000. According to Shchukin, et al. [5] a single vortex exists in the hemispherical dimple (h/D = 0,5 at $Re_D = 2260$, at $Re_D = 4520$ the vortex periodically changes the sign of rotation. In the Re_D number range from 9000 to 15500 the vortex transforms into the side-to-side oscillating pattern.

For an intermediate spherical dimple (h/D=0,13) the vortex angle slope is around 10 degrees with respect to a flat plate surface. The vortex structure persists downstream of a dimple a distance from 1,5 D to 2,5 D [9]. The analytical solutions and precise flow visualizations have disclosed “tornado-like” nature of the side-to-side fluctuating vortex with substantial in-vortex energy concentration [7].

These conclusions have been reported for the single spherical dimple with a sharp-edged rim. No side-to-side oscillating vortices were observed in a deep spherical dimple (h/D = 0,26) with a rounded-off rim [9], as well as in a deep dimple (h/D = 0,5) up to $Re_D = 350000$ at the supersonic (M< 4,0) flow [11]. Recent experiments [14, 15] have revealed that unsteady vortex structures also exist inside and downstream of a single shallow spherical dimple (h/D = 0,1) at relatively low Reynolds numbers ($Re_D < 25000$). Unlike high Re_D numbers, this type of flow unsteadiness is a bulk flow oscillation discharged from the dimple due to the in-dimple flow separation. The weak streamline fluctuations (Karman street type) downstream of a dimple appear as early as $Re_D \approx 3500$, transforming afterwards to bulk flow oscillations. The maximum of flow fluctuations (f = 13,4 Hz) is at $Re_D \approx 17500$, corresponding with a very high Strouhal number magnitude (Sh = 1,75) indicating the non-linear correlation between the freestream flow speed and bulk flow fluctuations.

Cylindrical dimples may be a good alternative to spherical dimples because of ease of manufacture. However, over the last few years there has not been much information added to the cylindrical single dimple database, which was established over 50 years ago by Wighardt [16]. The peaks in the drag increment curve $\Delta C_f = f(h/D)$ reflect important changes in the flow patterns. The minimum extra drag ΔC_f was found for shallow dimples at h/D from 0,1 to 0,2 and $h/\delta_o = 0,6$. Experimental data of Wighradt has shown the important role of relative boundary layer thickness on extra pressure losses. Terekhov, et al. [9] showed that unsteady flow structures exist inside a cylindrical dimple. Hiwada, et al. [17] demonstrated that a heat transfer minimum for both single spherical and cylindrical dimples is achieved at h/D = 0,2.

The Laser Doppler measurements were performed by Khalatov, et al. [15] to analyze the flow pattern after the shallow cylindrical dimple (h/D = 0,1) at relatively low Reynolds numbers ($Re_D < 23500$). Based on the boundary layer measurements an important conclusion has been made that the laminar-turbulent flow transition downstream of a cylindrical dimple (h/D = 0,1) occurs somewhere between $Re_D = 5200$ and 9400.

The shallow (h/D = 0,1) cylindrical dimples generate the bulk flow fluctuations in the downstream direction at $Re_D > 3500...4000$ with the maximum Strouhal number $Sh \approx 2,0$ reached at $Re_D \approx 9350$. The in-dimple reverse flow zone arises at $Re_D \approx 3500$ and steadily grows with Reynolds number increase. In addition, cylindrical dimples yield longer separation zones than spherical dimples given identical flow conditions. Asymmetrical dimples [2, 18, 19] generate the fluctuating vortex structures, as well, but additional investigations are necessary to study this in more detail.

There is a vast experimental database involving a rectangular dimpled channel. Ligrani, et al. [20] has given a brief review of these investigations. As reported [21], in a channel with tight dimple arrangement the key flow features responsible for the heat transfer augmentation over an array of dimples are: (a) shedding of multiple vortex pairs from dimples, (b) strong secondary fluid motions inside vortex pairs, (c) unsteadiness associated with vortex pair shedding and in-dimple flows. According to Ligrani, et al. [21], the vortex structures shed from the dimples become stronger as the ratio H*/D decreases. A primary vortex shedding frequency of 8,0 Hz and a dimple edge vortex pair oscillation frequency of 6,5 Hz have been detected for h/D=0,50 at $Re_H = 20000$ [22]. These frequencies are consistent with those obtained for the shallow single spherical and cylindrical dimples [14].

To summarize, the flow unsteadiness is an inherent flow feature of dimple configurations. The effect of flow unsteadiness on heat transfer and surface friction depends on the dimple configuration (spherical; cylindrical; asymmetrical; others), relative dimple depth (h/D), Reynolds numbers Re_D, and Rex (pre-dimple boundary layer thickness) numbers, and dimple rim shape (sharp-edged; rounded-off). A literature survey reveals that there have not been measurements of flow characteristics downstream of single dimple at various boundary layer thicknesses and relatively low Reynolds numbers where the effect of surface dimples is most significant.

OBJECTIVE

There is a very limited amount of information in the database for the relatively low flow velocity regimes corresponding to $Re_l < 25000$. The application of dimples for the flow separation control requires fundamental knowledge of the fluid flow features for the shallow dimples (h/D = 0,1) with different pre-dimple boundary layer thicknesses, simulating different dimple locations on the turbine blade.

The objective of this study is to investigate the details of the flow structures in front of, inside and after a shallow (h/D = 0,1) spherical and cylindrical dimple placed on a flat plate at different distances with different pre-dimple boundary layer thicknesses. The experimental study was performed under low Reynolds number conditions ($Re_D < 25000$) with a freestream pressure gradient of zero. This includes laminar flow pattern in front of the dimple, but both laminar and turbulent flow regimes after a dimple.

The results presented include the vortex patterns, in-dimple separation zone extent, unsteady flow phenomena (bulk flow oscillations), velocity profiles, and details of the laminar-turbulent flow transition downstream of the dimples. A comparison of both spherical and cylindrical dimple geometric configurations was made to assess their relative benefits.

EXPERIMENTAL FACILITY AND PROCEDURE

Test section

This experimental program was performed in the U.S. Air Force Academy (Colorado Springs) closed-circuit water tunnel (Fig. 1*a*) – capable of operating over a speed range of 0,05 m/s to 0,5 m/s with an axial flow pump capable of producing a volumetric flow rate of 0,7 m^3/s. The test channel is 1830 mm long with a rectangular cross section (610 mm height; 457 mm width). The sidewalls and floor (bottom) are made from a glass to allow for flow observation. The inlet nozzle has a contraction ratio of 6 : 1, the turbulence intensity at the test section inlet is below 1,0 %. The mean velocity at the inlet is uniform to within ± 2 %, the mean flow angularity is around ± 1,0 degrees in both pitch and yaw directions.

The general design of the test section has been considered in [14]. The test section (Fig. 1*b*) is an acrylic flat plate (19 mm thick) with an elliptically shaped leading edge (R ≈ 2 m). It is 1220 mm long and 381 mm wide. Two single cylindrical dimples separated in the spanwise direction were machined into the test section at a distance of 88 mm and 264 mm

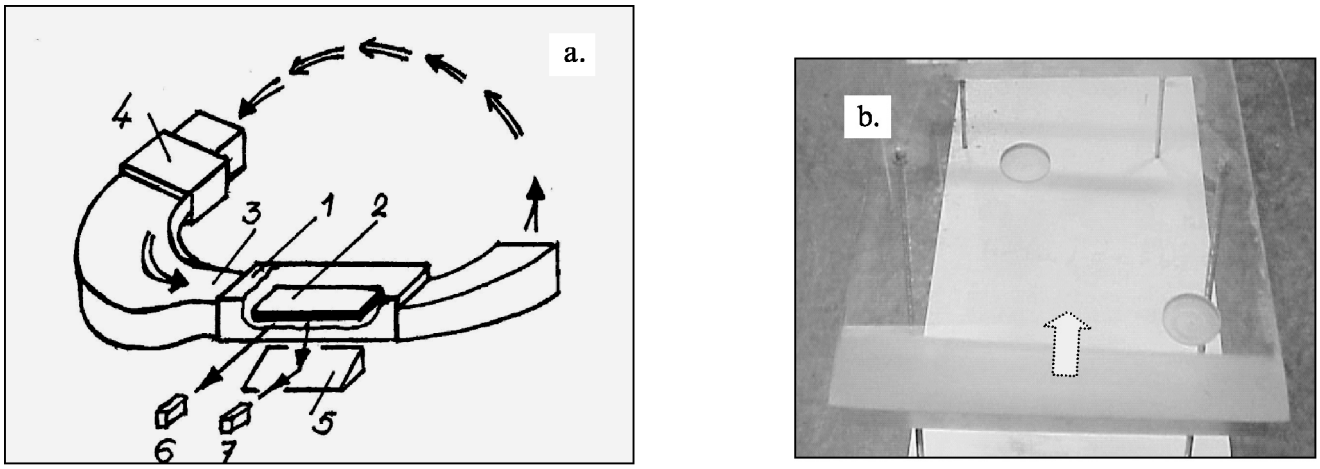

Figure 1. Schematic of the U.S. Air Force Academy Water Tunnel (a) and test section view (b). 1 – test channel. 2 – test section. 3 – inlet nozzle. 4 – axial flow pump. 5 – inclined floor mirror. 6 – digital camcorder (side observations). 7 – digital camcorder (top observations).

from the leading edge to the dimple center. Both dimples have the identical projected (surface) diameter of a dimple by means of a clay used to provide the inner fillet. The test cases and dimple locations are presented in Table 1.

The Reynolds number Re_D ranged from 3200 to 23500, corresponding to a range of Reynolds number Rex in front of the dimple leading edge of 3940 to 110450.

The dimpled flat plate in the test section was suspended upside down so that the flow structures could be observed through the transparent (glass) floor with the aid of an inclined mirror placed below the test channel. To visualize the flow structures, five different colors of dye were injected through five cylindrical ports machined both upstream and inside the dimple. A digital camcorder SONY-DCR VX2000 was used to record the flow patterns within and downstream of the dimple. A second camcorder was installed facing one of the side walls so that observations could be made from a side view perspective. All video images were stored as digital (AVI) files to allow computer screening at a reduced frame rate (slow motion) with Adobe Premiere 6,5 software. In this way the flow structures and patterns could be carefully observed, analyzed, and characterized. The TSI's two-dimensional Laser Doppler Velocimeter was employed to scan the boundary layer both in front and downstream of each dimple.

Table 1. Dimple parameters and test cases

No	Test case	h, mm	h/D	Distance to dimple leading edge, x	
1.	Single spherical dimple	5,08	0,10	88 mm, x/D=1,23	264 mm, x/D=4,7
2.	Single cylindrical dimple	5,08	0,10	88 mm, x/D=1,23	264 mm, x/D=4,7

Uncertainty Analysis

Using uncertainties of 1,2 mm for all dimensions of the test section, and a 1,0 % uncertainty for properties of water at 297 K, the uncertainty in Reynolds number was estimated to be within ± 2,4 %. Velocity measurements were calibrated to within ± 1,8 % using a video camera to record the time for a volume of dye to go the length of the test section (video camera frame rate is 29,97 frames per second). The frequency of the bulk flow oscillations was determined by counting the number of fluctuations shed by the dimple during a 15 sec interval. The uncertainty in frequency was estimated to be ± 10,6 %, which contributed to an uncertainty in the Strouhal number of ± 10,9 %. This occurred at the highest velocity, where the dye is diffused quickly making the fluctuations difficult to count even at a reduced video frame rate. At lower freestream velocities, both the frequency of fluctuations and the Strouhal number were more precise (as low as ± 3,66 % and ± 4,35 %, respectively).

Table 2. Boundary layer thickness data (flat plate)

No	x ,mm	Boundary layer thickness (LDV measurements)		Blasius solution
		Re_D	δ_0	δ_{00}
1.	63	4500	4,4	4,0
SCD		22240	1,5	1,71
2.	239	4500	6,0	7,56
SCD		22240	2,7	3,38

Table 3. Pre-dimple boundary layer thickness

No	x ,mm	Boundary layer thickness (LDV measurements)		Blasius solution
		Re_D	δ_0	δ_{00}
1.	63	4500	4,4	4,0
SCD		22240	1,5	1,71
2.	239	4500	6,0	7,56
SCD		22240	2,7	3,38

Finally, LDV measurements were estimated to be ± 3,5 %. The uncertainty in the extent of the separation zone inside the dimple is estimated to be within ± 7,8 % of the dimple diameter. All uncertainty estimates are based upon the methods of Coleman and Steele [23].

RESULTS AND DISCUSSIONS

Smooth flat plate

Before the dimples were machined into the plate, preliminary measurements were made over the smooth flat plate to characterize the primary flow parameters. The LDV system was employed to measure velocity profiles at locations of 63 mm and 239 mm downstream of the flat plate leading edge at potential dimple locations. The flow velocity in front of the test section was 0,099 m/s and 0,49 m/s giving the Reynolds numbers Re_D 4500 and 22240. The following primary conclusions have been drawn after the experimental data processing:

- The freestream velocity over the flat plate exceeded the inlet area-averaged velocity obtained by the volumetric flow meter by less than 3 %.
- At the lowest speed conditions the flow from x=0 to x=239 mm was slightly decelerating, while at the highest speed it was slightly accelerating from x = 0 to 150 mm. However, in both cases the freestream flow gradient factor f1 was far from the flow separation conditions.
- The pre-dimple boundary layer thickness data is given in Table 2. For the distance of x = 63 mm the difference between the measurements and calculations was within ± 14 %. At x = 239 mm the measured results are below the predictions by 26 %. The shape factor ratio H/H_{00} is equal to 1 ± 0,1 , where H_{00} is the value associated with the Blasius solution.

The primary conclusion is that between U_∞ = 0,099 m/s and 0,49 m/s the average flow parameters are fairly close to calculations obtained from the Blasius solution within the range of experimental uncertainty. However, the elliptically shaped leading edge provides small flow "distortions" up to the distance of x = 239 mm.

Pre-dimple flow parameters

Before the main experimental program, LDV measurements were performed in front of the cylindrical dimple ($x = x_D$) to identify the pre-dimple flow parameters. The flow fields were scanned upstream of the dimple front edge both on the dimple centerline and in the spanwise direction 0,25 D and 0,50 D off the centerline. Comparisons with the Blasius solution (Table 3) revealed some differences between measured and predicted values to be within ± 20 %. As concluded, it is due to effect of the elliptical leading edge generating the local gradient flow.

At x_D/D=0,66 upstream of the dimple and over the centerline (Fig. 2a) the axial velocity profile corresponds to the typical shear flow, however small reductions in the velocity profile can be seen above the boundary layer edge. Apparently, it is due to the convex curvature effect of the leading edge area. At the same upstream location but z = 0,25D off the centerline in the span wise direction (Fig. 2*b*), the effect of the in-dimple flow separation zone, unsteadiness, is present and the velocity profile experiences significant fluctuations. The average velocity profile, presented in Fig. 2b shows the "distortion zone" thickness is around 1 mm ($y/h \approx 0,2$). Further from the dimple centerline (z = 0,5 D), the velocity profile is close to the shear flow shape as given in Fig. 2*a*. At x_D/D = 4,04 along the centerline, the flow is the "pure" shear flow, however at z = 0,25 D offset

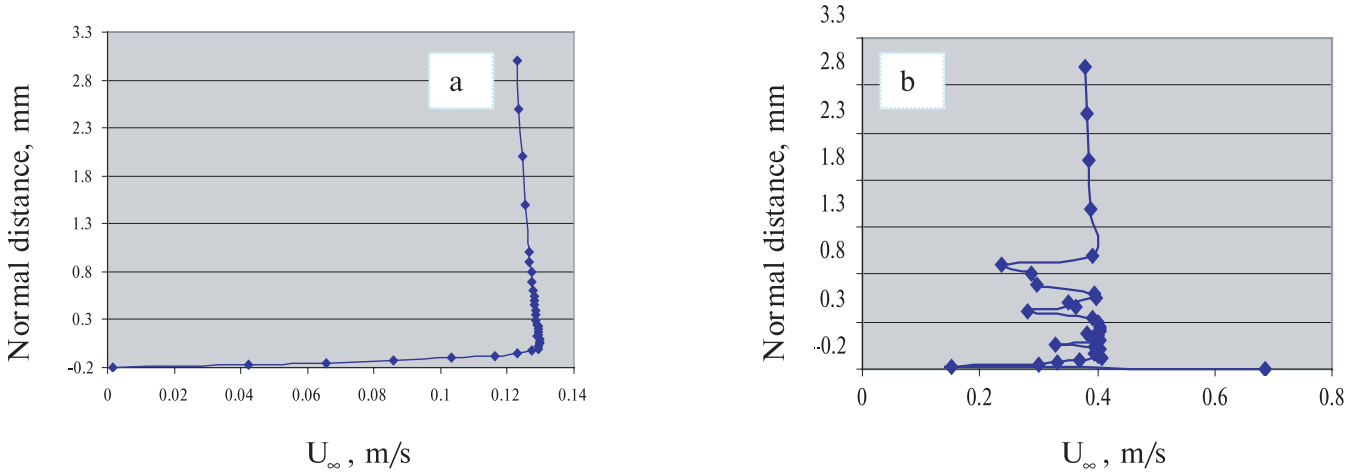

Figure 2. Average velocity in front of the cylindrical dimple (x_D/D=0,66). a: Dimple centerline. U_∞ = 0,115 m/s, Re_D=5220. b: 0,25 D spanwise offset. U_∞ = 0,36 m/s, Re_D = 16240.

location, the velocity "irregularities" occur up to y ≈ 2 mm (y/h ≈ 0,4). The shape factor H_{00} in front of the dimple varies from around 2,20 at x_D/D = 0,66 to 2,3...2,6 at x_D/D = 4,04. The lower H_{00} magnitude at x_D/D = 0,66 can be explained by the convex curvature effect of the elliptical leading edge area. The conclusion is that a laminar flow pattern occurs in front of the dimple (centerline) at all flow regimes studied.

SINGLE CYLINDRICAL DIMPLE

Flow pattern (x/D=1,23)

Details of the flow patterns obtained from visualizations have been considered in depth in [14]. Fluctuations of the centerline streamlines and 0,25 D offset streamlines become clear starting at Re_D = 3200 accompanied with periodic bulk flow fluctuations over the dimple axis. The region of in-dimple separated flow formed at Re_D = 3200 and grew rapidly up to Re_D ≈ 8000, where the length of the separation zone is around 0,45 D. The twin vortex appears at Re_D ≈ 4100 and grows to Re_D = 9300, where the maximum bulk flow oscillations were found. At Re_D = 9300 the extent of the separation zone (0,45 D) is identical at both the centerline and at the 0,25 D offset. For Re_D >6600 both 0,50 D offset streamlines were drawn into the dimple space. The rate of the twin vortex rotation increased with Reynolds number. At Re_D = 15100 the legs of the twin vortex changed the sign of their rotation and created a new vortex pair configuration with diverging flow at the separation line. The extent of the separation zone grew to 0,73 D at Re_D = 23450.

Flow pattern (x/D=4,70)

Measurements further downstream indicate that an increase in the boundary layer thickness greatly influences the flow pattern inside and downstream of a dimple. Starting at Re_D = 3200 the flow structure becomes unsteady and alternates. The small size and weakly fluctuating separation bubble was formed behind the downstream dimple rim transforming periodically into the wide wake flow pattern downstream of the dimple. At Re_D > 8,000 the flow continued to alternate however it demonstrated an asymmetric wake pattern. As expected, this is the beginning of the turbulent flow formation inside the dimple. Starting at Re_D = 12200 the separated flow forming inside the dimple accompanied the symmetrical wake downstream of the dimple. The separation zone grows monotonically up to Re_D = 23500, where the separation zone extent is around 0,45 D. This is however 70 % smaller than that for the dimple at x/D = 1,23 and the same Re_D number. Inside the non-separated zone the flow streamlines are very irregular. Starting at Re_D = 18000 the weak twin vortex type flow forms inside the dimple and grows slowly up to Re_D =23500.

The periodic and stable bulk flow fluctuations downstream of the dimple began at Re_D > 10000. These fluctuations are considerably lower than that observed for the cylindrical dimple at x/D=1,23. At

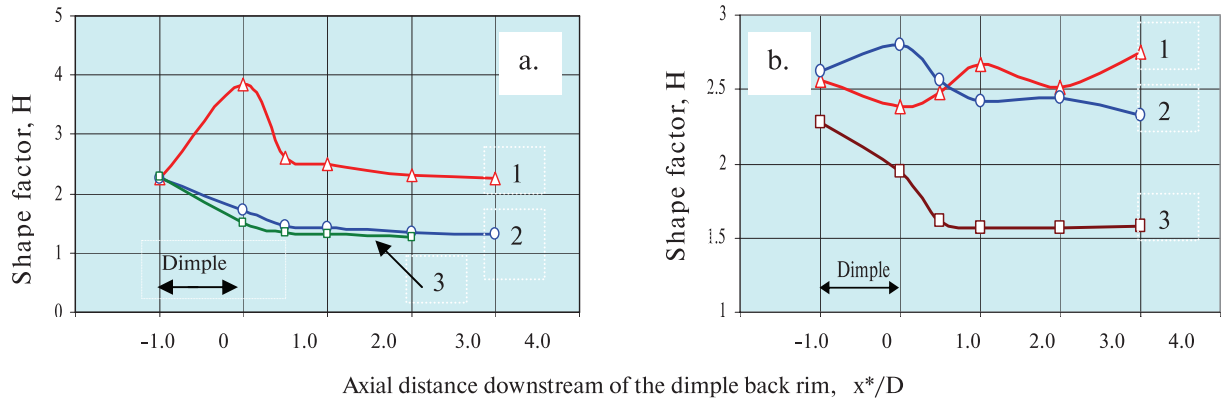

Figure 3. Shape factor H in front and downstream of cylindrical dimple. a: x/D = 1,23. b: x/D = 4,70. 1 – Re_D = 5220. 2 – Re_D = 9430. 3 – Re_D = 16240.

Re_D > 16500 the bulk fluctuations for both locations (x/D = 1,23 and x/D = 4,7) are actually the same which indicates that the pre-dimple boundary layer thickness had little effect.

Flow fields downstream of the dimple

All measurements were performed over the centerline downstream of the dimple. The inlet area-averaged flow speed U_∞varied from 0,115 m/s to 0,36 m/s giving the ReD number range of 5220 to 16240. The LDV scanning of the boundary layer was performed at the non-dimensional distance of x*/D = 0; 0,50; 1,0; 2,0, and 3,0 downstream of the rear dimple rim. The following conclusions have been drawn from the measurements.

- **x/D=1,23.** At the low flow speed a small area of reduced speed (1 mm thick) arose immediately after of the dimple. The 1 mm thick "kink" is not a flow separation yet, but demonstrates the interaction of "free" flow over a dimple and "back step" of the rear dimple rim. At x*/D=0,5 and x*/D=2,0 the velocity profile near the wall was close to the linear law indicating the laminar flow pattern. At the highest speed a turbulent flow pattern arose immediately downstream of the dimple which was maintained further downstream. No flow separation was found over the entire plate surface downstream of the dimple. Therefore, at x*/D=1,23 the laminar-turbulent flow transition occurs between Re_D =5220 and 9430, where the δ_{0av}/h magnitude is 0,39 as follows from Table 3. Here $\delta_{0av}$is the average boundary layer thickness δ_0 between Re_D = 5220 and 9430.
- **x/D=4,70.** At the low and middle flow speeds a weak separation zone arose at x*=0, however at x*/D>0,5 the laminar flow existed over the remainder of the flat plate. At the highest flow speed a separation zone begins at x*= 0 followed by a turbulent flow pattern at x*/D>0,5. In this case, the transition to turbulent flow occurs between Re_D = 9430 and 16240 with δ_{0av}/h =0,98. Thus, the increase in the pre-dimple boundary layer thickness increased Reynolds number ReD where the laminar-turbulent flow transition finally took place.

Conclusions yielded from this data are consistent with the measured shape factor distributions presented in Fig. 3. As a first approach, one may conclude that for δ_{0av}/h=0,39 transition to the turbulent flow occurs at $Re_D \approx 7235$ (average value between two "borders"), while for δ_{0av}/h = 0,98 this occurs at $Re_D \approx 12835$.

The flow that reaches the edge of a cylindrical dimple sees a more abrupt drop off than for the flow approaching a spherical indentation back rim. For the flow along the dimple centerline, it is much more like flow over a backward facing step. For the spherical dimple, the rim of which is 'smoother", the laminar-turbulent flow transition may occur at greater Re_D numbers then found for the cylindrical dimple.

SINGLE SPHERICAL DIMPLE

Flow pattern (x/D=1,23)

The flow patterns have been discussed in detail in [14]. At low velocities (Re_D = 3300...4200) all streamlines over the dimple were quite parallel and only small fluctuations at (1,4 to 1,8 Hz) were observed along the center streamline. These fluctuations were

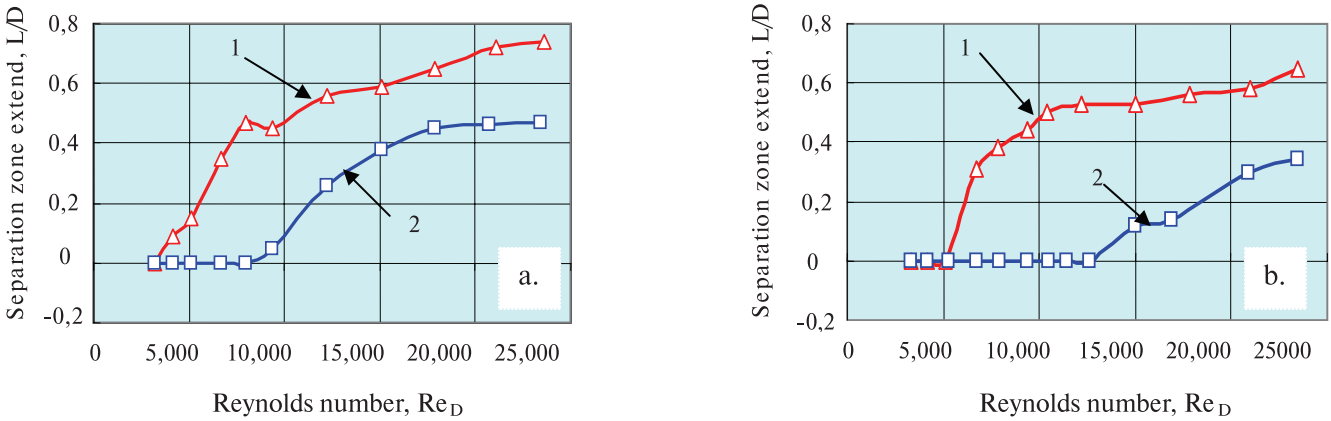

Figure 4. Extent of the in-dimple separation zone over centerline: cylindrical (a) and spherical (b) dimple. 1 – x/D = 1,23. 2 – x/D = 4,70.

confined to a small zone near the downstream edge of the dimple. As Re_D was increased to 5,200, a separation zone began to form inside the dimple along the downstream edge. At Re_D > 6700 there was a slow and periodically alternating clockwise and counter-clockwise bulk flow rotation inside the dimple with an accompanying periodic migration of the separation zone between the dimple centerline and the streamline offset from the centerline by 0,5 D. These rotational fluctuations ceased at Re_D = 12200 at which point the separation zone became symmetrical with respect to the dimple centerline. At Re_D = 7900, a weak twin vortex appeared inside the non-separated zone inside the dimple. Thus, between Re_D = 12200 and Re_D = 21000, the flow inside the dimple included both a twin vortex and a region of separation. Finally, as Re_D was increased to 23450, the separation zone inside a dimple became very large, which led to the elimination of the twin vortex structure. Only chaotic streamlines could be seen within the non-separated zone near the upstream edge of the dimple. The maximum frequency of bulk flow fluctuations (f = 13,4 Hz) was found at Re_D = 17900.

Flow pattern (x/D=4,70)

At low velocities and up to Re_D = 10500 the flow downstream of the dimple was of the "strip type" transforming into asymmetrical wake flow at Re_D = 11400. An asymmetrical wake with a small separation bubble existed until Re_D=16900, e.g. much longer than for the single spherical dimple located at x/D=1,23 (lower δ_0/h value). The fully developed symmetrical flow after the dimple formed only after Re_D >17000. However, the length of the in-dimple separation zone was much smaller than for the dimple located at x/D=1,23. The maximum separation zone length was 0,35 D which was roughly half the size of the zone for the dimple at x/D=1,23.

The bulk flow fluctuations downstream of the spherical dimple became visible and regular only above $Re_D \approx 9000$. Above this point the flow fluctuations grew very rapidly and reached the maximum Strouhal number at $Re_D \approx 17000$. This occurred while there were the asymmetrical structures downstream of the dimple. As a whole, in the Reynolds number range of 10000 to 17000, the Strouhal number is of 40 % to 50 % lower of that for the dimple located at x/D =1,23. Over $Re_D \approx 24000$, there is no effect of the boundary layer thickness on the downstream bulk flow fluctuations and the Strouhal numbers are virtually identical for both spherical dimples located at x/D=1,23 and x/D=4,70 at this elevated Re_D.

IN-DIMPLE SEPARATION ZONE EXTENT

The average length of the separated region L inside the dimple was measured along the dimple centerline. This length is the distance between the beginning of the separated region and the downstream rim of the dimple. The data taken from a few "frozen" video images for the same Reynolds number was averaged and presented in Fig. 4 as the non-dimensional length L/D of the separated region plotted versus Re_D number. At x/D =1,23 (low δ_0/h value) for the cylindrical dimple the flow separation began at $Re_D \approx 3500$, while for the spherical dimple it originated at

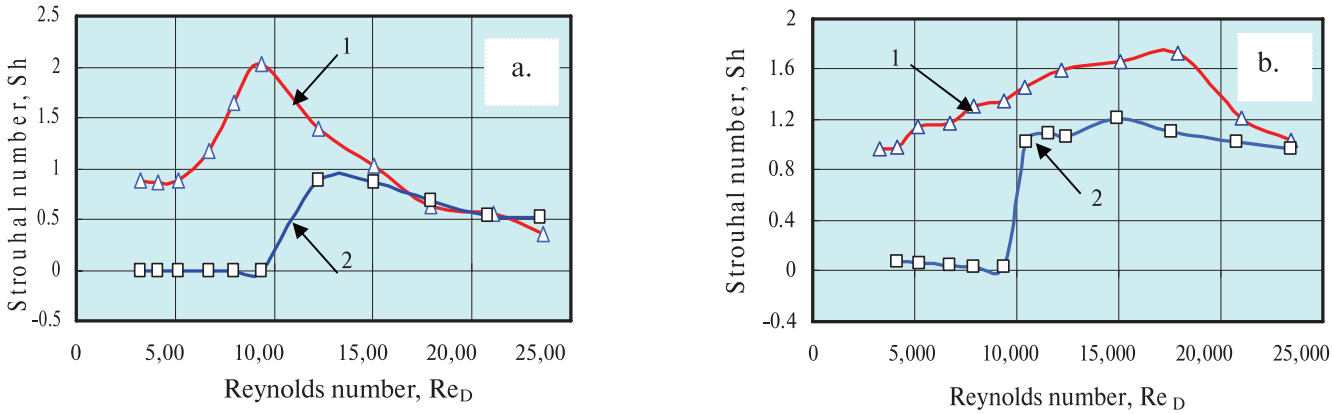

Figure 5. Bulk flow oscillations beyond cylindrical (a) and spherical (b) dimple. 1 – x/D = 1,23. 2 – x/D = 4,70.

$Re_D \approx 5200$. In both cases the extent of the separation zone increased monotonically as Re_D increased, but more appreciably between $Re_D = 5500$ and 10000. For the cylindrical dimple the length of the separated zone was slightly greater than that of the spherical dimple. Increase in the boundary layer thickness (x/D = 4,7) reduced the separation zone more appreciably for the spherical dimple. Also, the growth of δ_0/h delayed the formation of the separation zone to higher Reynolds numbers.

BULK FLOW FLUCTUATIONS

Preliminary experiments documented in [14] have identified suitable locations for the video camcorder so that the bulk flow oscillations could be clearly observed and recorded. As reported, the experimental data taken from three independent test set-ups (top view: dye injection in front of, and inside a dimple; side view) yielded about the same value of Strouhal numbers across a wide range of Reynolds numbers. All three were used in subsequent measurements as a check for consistency. Figure 5 is a plot of the local Strouhal number versus the Reynolds number Re_D for different dimple locations. This correlation determines the bulk flow oscillations downstream of the dimple.

For all cases, the Strouhal number curve reaches a maximum value at a certain Reynolds number and then drops off at higher Re_D. The lower the pre-dimple boundary layer thickness δ_0/h, the higher the Strouhal number. The cylindrical dimple at x/D=1,23 and $Re_D < 12000$ creates higher bulk flow oscillations than the corresponding spherical dimple. At x/D=4,7 the spherical dimple data exceeds cylindrical dimple results. As a whole increases in the boundary layer thickness in front of a dimple reduces the bulk flow oscillations. Moreover, the Strouhal number maximum relates to the greater Reynolds numbers for cylindrical dimples and to the lower Reynolds numbers for the spherical dimples. No effect from the boundary layer thickness was apparent for the cylindrical dimples at $Re_D > 16500$ and for the spherical dimple at $Re_D > 24000$.

Comparison of Figs 4 and 5 reveals that the spherical dimple generates fluctuations even when there is no separation zone. However, these fluctuations are very small and located only in the narrow area next to the axis. For the cylindrical dimple, the beginning of the separation zone roughly coincides with considerable growth of bulk flow oscillations.

The rapid growth of Strouhal number occurs immediately after the separation zone appears and develops. In turn, the present study has shown the separation zone extent is a function of the dimple shape (spherical; cylindrical) and pre-dimple boundary layer thickness δ_0/h.

It seems the latter determines the ratio of a flow mass situated in front of and inside a dimple. At low δ_0/h, this ratio is too small to prevent the flow separation and fluctuations inside the dimple, however at higher δ_0/h the higher mass of external flow "suppresses" the bulk flow oscillations.

CONCLUSIONS

1. The flow pattern inside of and downstream of spherical and cylindrical dimples is inherently a

three-dimensional and unsteady flow with downstream bulk flow fluctuations. An increase in the relative boundary layer thickness (x/D growth) leads to the onset of the specific flow patterns.

2. The dimple influences upstream flow parameters, mostly appreciably at 0,25D offset of the dimple centerline in the spanwise direction. These unsteady distortions in the velocity profile are due to the influence of the in-dimple separated flow which is propagated upstream.

3. An increase in the pre-dimple boundary layer thickness reduces the extent of the in-dimple separation zone and the intensity of bulk flow fluctuations. The rate of bulk flow fluctuations is in sync with in-dimple separation zone growth.

4. No effects from the boundary layer thickness were found for the cylindrical and spherical dimples at Re_D>16500 and Re_D>24000 respectively.

5. The bulk flow oscillations "activate" the laminar-turbulent flow transition, the lower the relative boundary layer thickness, lower critical Reynolds number.

6. The next target is studying of one and two spanwise row of dimples relevant to flow separation control technique and heat transfer augmentation.

ACKNOWLEDGMENTS

This research was performed while visit of Prof. A. Khalatov to the Aeronautics Laboratory of the U.S. Air Force Academy in Colorado Springs. The partial support of CRDF Grant # UE2-552-KV-02, Collaborative NATO Linkage Grant # PST.CLG.979702 (2003-2005) is also acknowledged.

REFERENCES

1. *Lake J.P., King P.I., Rivir R.B.* Low Reynolds Number Loss Reduction on Turbine Blades with Dimples and V-Grooves // AIAA Paper 2000-738. 2000.

2. *Rouser K.* Use of Dimples to Suppress Boundary Layer Separation on a Low Pressure Turbine Blade. – M.S. Thesis, Air Force Institute of Technology, 2002, WPAFB, Ohio, USA.

3. *Кикнадзе Г.И., Гачечиладзе И.А., Олейников В.Г., Алексеев В.В.* Механизмы смерчевой интенсификации тепломассообмена // Труды 1-ой Российской национальной конференции по тепломассобмену. – Москва: Изд. МЭИ. – 1994. – Т. 8. – С. 97 – 106.

4. *Афанасьев В.Н., Чудновский Я.П.* Экспериментальное исследование структуры течения в одиночной впадине // Москва: Вестник МГТУ. – Сер. Машиностроение. – 1993. – №4. – С.85 – 95.

5. *Щукин В.К., Козлов А.П., Чудновский Я.П., Агачев Р.С.* Интенсификация теплообмена сферическими лунками // Доклады РАН. – Сер. Энергетика. – 1998. – No 3. – С.47 – 64.

6. *Нагога Г.П.* Эффективные способы охлаждения лопаток высокотемпературных газовых турбин. – М: Изд. МАИ, 1996. – 99с.

7. *Гачечиладзе И.А.* Теплообмен при самоорганизации вихревых структур. – В книге: "Тепло- и массобмен. Конвективный теплообмен (Проблемные доклады)". – Минск: Изд. ИТМО АН БССР. – 1988. С.83 – 125.

8. *Терехов В.И., Калинина С.В., Мшвидобадзе Ю.М.* Теплоотдача от каверны сферической формы, расположенной на стенке прямоугольного канала // Теплофизика высоких температур. – 1994. – Т. 32. – No 2. – С.249 – 254.

9. *Терехов В.И., Калинина С.В., Мшвидобадзе Ю.М.* Теплоотдача от сферической лунки, расположенной в следе другой лунки // Теплофизика и аэромеханика. – Сибирское Отделение РАН. – 2001. – Т. 8. – No 2. – С.237 – 242.

10. *Езерский А.Б., Шехов В.Г.* Тепловая визуализация потока около единичной лунки // Известия РАН. – Механика жидкости и газа. – 1989. – No 6. – С.161 – 164.

11. *Боровой В.А., Яковлев Л.В.* Теплообмен в единичном углублении при сверхзвуковом обтекании // Известия РАН. – Механика жидкости и газа. – 1993. – No 5. – С.48 – 52.

12. *Кесарев В.С., Козлов А.П.* Структура течения и теплообмен при обтекании полусферического углубления турбулизированным потоком воздуха // Москва: Вестник МГТУ. – Сер. Машиностроение. – Москва. – 1993. – No1. – С. 106–115.

13. *Snedeker R.S., Donaldson C.P.* Observation of a Bi-stable Flow in a Hemispherical Cavity // AIAA Journal. – Vol. 4. – No 4. – 1966.

14. *Khalatov A.A., Byerley A., Seong-Ki Min, Ochoa D.* Flow Characteristics Within and

Downstream of Spherical and Cylindrical Dimple on a Flat Plate at Low Reynolds Numbers // ASME Paper No GT2004-53656. 2004.

15. *Khalatov A.A., Byerley A., Seong-Ki Min & Vincent R.* Application of Advanced Techniques to Study Fluid Flow and Heat Transfer Within and Downstream of a Single Dimple // Материалы 5-го Международного форума по тепло- и массообмену. Минск: Изд-во ИТМО АНБ. – 2004. – С. 1–20 (англ.).

16. *Wighart K.* Erhohung des Turbulenten Reibungswidestandes Durch Oberflachen-Storungen // Forschungshefte fur Schiffstechnikю – 1953. – No 1. – pp. 65– 81.

17. *Hiwada M., Kawamura T., Mbuch J., & Kumada M.* Some Characteristics of Flow Pattern and Heat Transfer Past a Cylindrical Cavity // Bulletin of JSME. – 1983. – Vol. 26. – No 220. – pp. 1744 –1758.

18. *Kovalenko G.V., Khalatov A.A.* Fluid Flow and Heat Transfer Features at a Cross-Flow of Dimpled Tubes in a Confined Space // ASME Paper No GT2003-38155. 2003.

19. *Isaev S.A., Leont'ev A.I., Zhdanov V.I.* Simulation of Tornado-Like Heat Transfer at Flow Passing a Relief with Dimples // Heat Transfer-2002. – Proceedings of 12th International Heat Transfer Conference. Grenoble, France. – pp. 735–738.

20. *Ligrani P.M., Oliveira M.M., Blaskovich T.* Comparison of Heat Augmentation Techniques // AIAA Journal. – 2003. – Vol. 41. – No 3. – pp. 337–362.

21. *Ligrani P.M., Harrison J.L., Mahmood G.I., Hill M.L.* Flow Structure due to Dimple Depression on a Channel Surface // Physics of Fluids. – 2001. – Vol.13. – No11. – pp. 3442–3451.

22. *Burgess N.K., Ligrani P.M.* Effects of Dimple Depth on Nusselt Numbers and Friction Factors for Internal Cooling in a Channel // ASME Paper No GT2004-54232. 2004.

23. *Coleman H., Steele G.* Experimentation and Uncertainty Analysis for Engineers. -John Wiley & Sons. New York, NY. 2d Edition. – 1999. – 275p.

Получено 13.07.2006 г.

УДК 629.12.03

Басок Б.И., Рыжков С.С.

Институт технической теплофизики НАН Украины

ИССЛЕДОВАНИЕ ВЛИЯНИЯ НЕИЗОТЕРМИЧНОСТИ ПЛОСКОГО КАНАЛА НА ХАРАКТЕРИСТИКИ ДИСПЕРСНОГО ДВУХФАЗНОГО ПОТОКА

Виконано розрахунок основних теплофізичних та гідродинамічних характеристик дисперсного двофазного середовища для гладкого каналу в тривимірній постановці. Встановлено відсутність впливу перепаду температур до 80 °С на розподіл швидкості, кінетичної енергії турбулентності і статичного тиску та встановлено вплив на концентрацію дисперсної фази двофазного середовища в каналі. Основне зниження концентрації дисперсної фази двофазного середовища (більше 95 %) відбувається за рахунок осадження часток на верхній і нижній стінках каналу. Осад-

Выполнен расчет основных теплофизических и гидродинамических характеристик дисперсной двухфазной среды для гладкого канала в трехмерной постановке. Установлено отсутствие влияния перепада температур до 80 °С на распределение скорости, кинетической энергии турбулентности и статического давления, и установлено влияние на концентрацию дисперсной фазы двухфазной среды в канале. Основное снижение концентрации дисперсной фазы двухфазной среды (более 95 %) происходит за счет осаждения частиц на верхней и нижней

Research of main thermalphysic and hydrodynamic characteristics of disperse dysphasic environment for the flat 3-D channel has been executed. Temperature drop –up to 80 °С do not influence on velocity distribution, Turbulent kinetic energy, static pressure but influence on concentration of disperse dysphasic environment in the channel. Main concentration decrease of disperse dysphasic environment (up to 95%) happens with the help of particles sedimentation on the up and down channel walls. Sedimentation on the back wall could not be taken into consideration and it is pos-